A three-dimensional multi-physics model for a Li-ion battery

Meng Guo [a], Gi-Heon Kim [b], Ralph E. White [a,*]

[a] Department of Chemical Engineering, University of South Carolina, Columbia, SC 29208, USA
[b] National Renewable Energy Laboratory, Golden, CO 80401, USA

HIGHLIGHTS

- A 3D multi-physics model for a lithium-ion battery module with three cells in series is developed.
- This model is used to predict the distributed electrical/thermal behavior of the battery.
- A physics-based pseudo-2D model is used to describe the electrochemical behavior.

ARTICLE INFO

ABSTRACT

A multi-geometry and multi-physics model is developed for a Li-ion battery module which includes three cells connected in series by electrical busbars. The model can be used to predict the 3D profiles of the electrical potentials and temperature in the battery. The physics-based porous electrode (P2D) model is used to predict the electrochemical behavior of the cells, and the coupling between the P2D model and the electrical/thermal equations is simplified through a linear approximation method. This approximation is useful at rates of at least 5 C and reduces the computation time significantly. The anisotropic conductive properties for the regions where conductors are separately arrayed are discussed in detail, and the model predictions are presented and discussed.

1. Introduction

Currently, as battery packs including multiple large-format Li-ion cells are widely used in the hybrid electrical vehicles (HEV) and space craft [1,2], there is an increasing demand for computer-aided tools that enable the battery community to design and simulate batteries. These software tools are expected to have access to the latest numerical methods and algorithms and facilitate battery design by integrating battery modeling components within an open architecture. Therefore, a standardized model template which can capture most physical features of cells and batteries and be implemented within an open architecture would be ideal to meet such demands.

As the thermal and electrical behavior is quite non-uniform through the cells during the charge/discharge operations at high-current rates [3–6], multi-dimensional and multi-physics models are usually suggested for large-format batteries. In recent years,

various multi-dimensional mathematical models and model order reduction approaches have been proposed to simulate effectively the distributed thermal, electrical, and electrochemical behavior within an electrode plate pair or a single cell [7–15]. However, very little work has been reported concerning the 3D multi-physics modeling for large batteries.

The huge computational load is one of the major problems that prevents the single-cell-level models from being extended to the multi-cell-level, especially for those cell models including the full-order physics-based electrochemical sub-models [16–18]. In the most recent work of our research group, a very efficient model simplification method, the linear approximation method [19], was developed based on a two-dimensional electrode plate pair domain; the linear model developed with this method can be used to simulate the charge/discharge operations using only a few seconds of computation time; and the thermal/electrical results from the linear model agree well with the results from the full-distribution model which requires about 1000 times more computation time than the linear approximation method. Another issue in developing this 3D battery model is the difficulty in identifying the transport properties in the connecting regions between the cell electrodes and external parts. The current collectors of

* Corresponding author. 301 Main Street, Columbia, SC 29208, USA. Tel.: +1 803 777 3270.
  E-mail address: white@cec.sc.edu (R.E. White).

electrodes are connected to the external parts through many thin metal foils arrayed in complex patterns, and the apparent thermal/electrical conductive parameters in these connecting regions vary significantly with position. No literature report has been found so far on how to evaluate these anisotropic transport phenomena.

Our research group is currently working on the solutions for those above-mentioned problems. In the first step, our goal is to develop a three-dimensional multi-physics model template using the linear approximation approach presented in Ref. [19]. In this model template, a battery module including multiple cells is divided into different computational domains according to the transport and reactive properties and the general electric and thermal equations are specified in each domain. It is noted that we have found a way to identify the transport properties in the connecting regions between the cell electrodes and external parts based on basic geometry relations. The governing equations and inputs are standardized and users can implement this model with different commercial or non-commercial software for various simulation purposes. The details of the model development and the simulation results are presented in this paper, and extended research will be covered in our future work.

2. Mathematical model

2.1. Configuration of battery module

The battery module presented in this paper includes three Li-ion pouch cells connected in series (3S module) through two electric busbars. The geometry and electrical circuit diagram for this 3S module are presented in Fig. 1. Each single pouch cell forming this module is divided into different parts in terms of electrical and thermal conducting properties. In the electroactive region of each cell, current and electrochemical heat sources are included and the conductive current flows only in the two planar directions (in the x–z plane) along the current collector foils; the thermal conductivity in the transversal direction (the y direction) is much smaller than in the planar directions because the y direction heat flux goes through the less-conductive separator layers. The lower parts of the electrode tabs are labeled as the tab bases, where the current collector conductor foils extend separately from the current collector in the electroactive regions of the cells to the tab terminals. The upper parts of electrode tabs, which are labeled as the tab terminals, have isotropic properties and are connected to the electric busbars or serve as the inlet/outlet for the applied current. The dimensions for the cells are shown in Fig. 2, the thickness of each cell (d_{Cell}) is 9 mm, the distance between two adjacent cells (Δ_{Cell}) in the module is 27 mm, the thickness for the positive and negative electrode tab terminals (d_{Tab}) are respectively 0.375 mm and 0.24 mm, and the thickness of the busbar (d_{BB}) is 1 mm.

2.2. Definitions of reference and modified electric potentials

In this model, four reference electric potentials, V_0, V_1, V_2, and V_3, are defined at different locations as shown in Fig. 3; where V_0 is set to zero, while $V_1(t)$, $V_2(t)$, and $V_3(t)$ are state variables which change only with time.

In this model, two modified electric potentials, Φ_L and Φ_R, are defined throughout the module domains (as shown in Table 1). The modified potentials are expressed as the difference between the actual potential (Φ_+, Φ_-, or Φ) and the reference potential in each conductive domain. Details for the definitions of modified potential in different domains are presented in Table 1, where Φ_+ and Φ_- are the actual potentials of the positive and negative electrode current collectors and tabs, and Φ is the actual potential of the busbars. According to the definitions, the modified potentials are zero at locations chosen for the reference potentials, and these constraints are used as imposed limiting conditions to obtain solutions for the electrical equations.
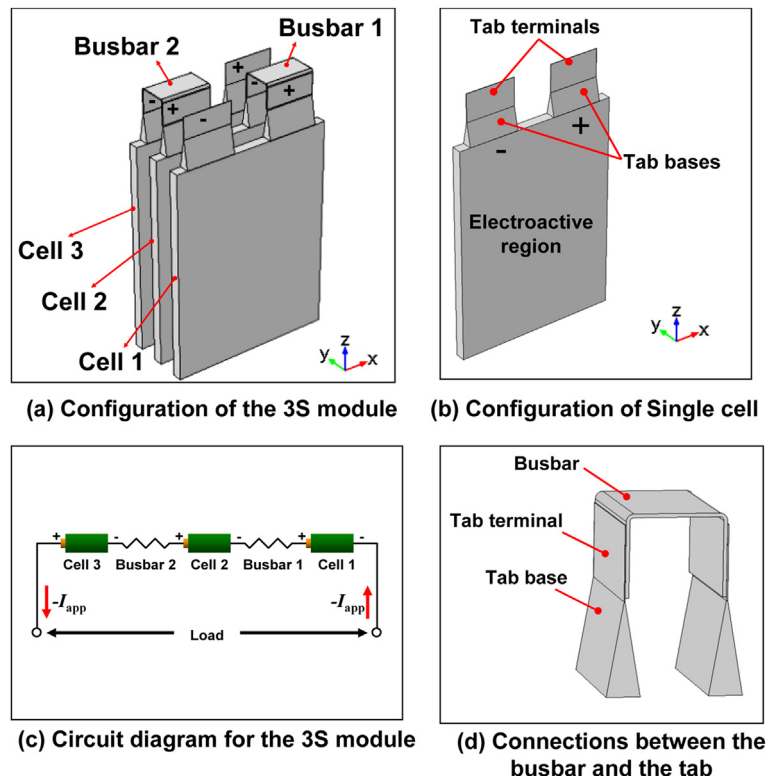

(a) Configuration of the 3S module

(b) Configuration of Single cell

(c) Circuit diagram for the 3S module

(d) Connections between the busbar and the tab

Fig. 1. Configuration and circuit diagram for the 3S battery module.
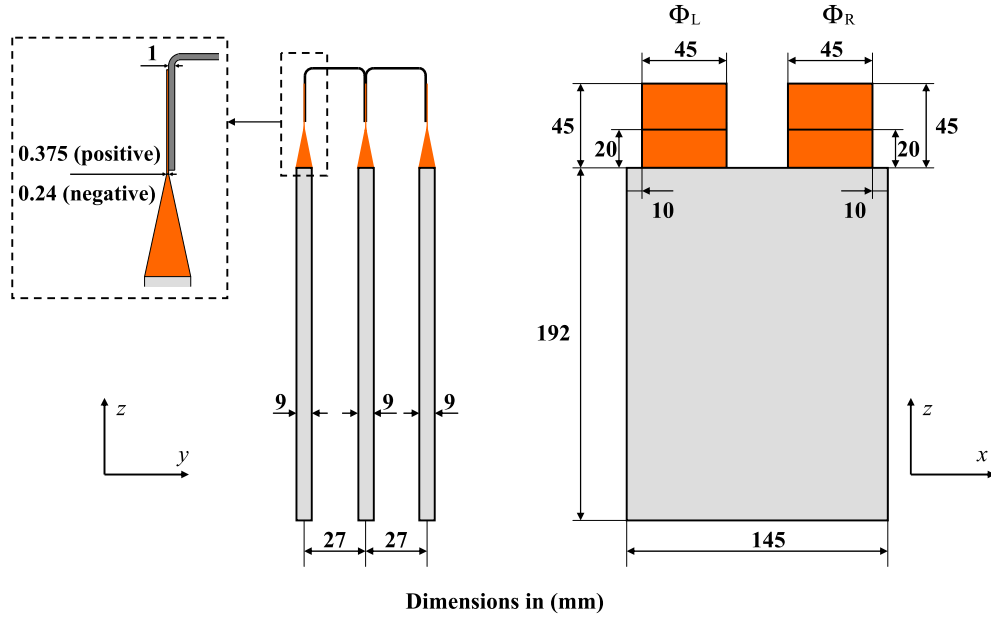
Dimensions in (mm)

Fig. 2. Dimensions of cell.

2.3. Electrical and thermal equations

2.3.1. General form

The general form of the electrical equation is expressed as:

$$-\nabla \cdot \left(-\underline{\underline{\sigma}} \nabla \Phi_j \right) + i_V = 0 \quad (j = L, R) \tag{1}$$

where $\underline{\underline{\sigma}}$ is the matrix for electrical conductivities of the domain materials and i_V is the volumetric current source. The general form of the thermal equation is expressed as follows:

$$\rho C_P \frac{\partial T}{\partial t} = -\nabla \cdot \left(-\underline{\underline{k}} \nabla T \right) + Q_V \tag{2}$$

where ρ and C_P are, respectively, the density and specific heat capacity of the domain material, $\underline{\underline{k}}$ is the matrix for the thermal conductivities of the domain material, and Q_V is the volumetric heat source.

#### 2.3.2. Tab terminals and busbars

The tab terminals and electrical busbars are isotropic conductors where only one modified potential is defined; therefore the thermal and electrical conductivities in these domains are scalars:

$$\underline{\underline{\sigma}} = [\sigma_c] \tag{3}$$

$$\underline{\underline{k}} = [k_c] \tag{4}$$

where σ_c and k_c are, respectively, the electrical and thermal conductivities of the domain material. The volumetric current source term, i_V, is zero in the tab terminals and busbars. Joule heating is the only heat source in the tab terminal and busbar domains; therefore, the volumetric heat source term Q_V is expressed as:

$$Q_V = \left(-\underline{\underline{\sigma}} \nabla \Phi_j \right) \cdot \left(-\nabla \Phi_j \right) \quad (j = L, R) \tag{5}$$
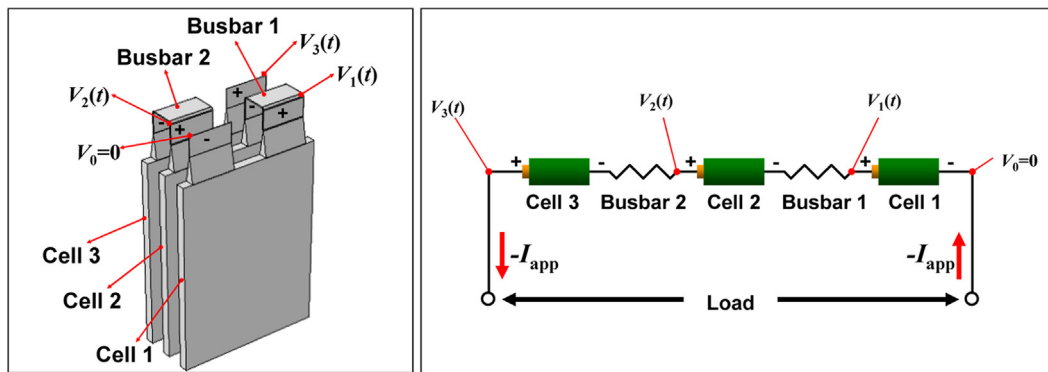
(a) Locations of reference potentials in the modeling domain

(b) Locations of reference potentials in the circuit diagram

Fig. 3. Reference potentials (v_0, $v_1(t)$, $v_2(t)$, and $v_3(t)$) defined at different locations.

Table 1
Definitions of modified potentials.

		Definition of Φ_L	Definition of Φ_R
Cell 1 (negative electrode tab at the left)	Electroactive region	Φ_-	$\Phi_+ - V_1(t)$
	Positive electrode tab	Not defined	$\Phi_+ - V_1(t)$
	Negative electrode tab	Φ_-	Not defined
Busbar 1		Not defined	$\Phi - V_1(t)$
Cell 2 (negative electrode tab at the right)	Electroactive region	$\Phi_+ - V_2(t)$	$\Phi_- - V_1(t)$
	Positive electrode tab	$\Phi_+ - V_2(t)$	Not defined
	Negative electrode tab	Not defined	$\Phi_- - V_1(t)$
Busbar 2		$\Phi - V_2(t)$	Not defined
Cell 3 (negative electrode tab at the left)	Electroactive region	$\Phi_- - V_2(t)$	$\Phi_+ - V_3(t)$
	Positive electrode tab	Not defined	$\Phi_+ - V_3(t)$
	Negative electrode tab	$\Phi_- - V_2(t)$	Not defined

2.3.3. Tab bases

As shown in Fig. 4 (also in Appendix A), in a tab base, many current collector conductor foils are arrayed in radial arrangements and there are spaces between the individual foils. The tab base domain can be modeled as a porous media (foils and air) where the bulk density of the domain material is expressed as:

$$\rho = \varepsilon_c \rho_c \qquad (6)$$

where ε_c is the volume fraction of conductor foils in the tab base and ρ_c is the actual density of the conductor foil. The value of ε_c changes with location, and the expression for this term is derived in Appendix A.

Since the conductor foils in the tab bases do not contact each other, the conductive current only flows through some specific planes where the conductor foils are located and there is no current flow in the directions normal to these conductor foil planes. Similarly, the heat transfer rates in the spaces between the conductor foils are very small and the normal direction heat flux in the

Fig. 4. The y–z plane cross section of the tab base.

conductor foil planes can also be neglected. Therefore, the tab bases exhibit anisotropic electrical and thermal conductive properties. The matrices for thermal and electrical conductivities in the tab base domains can be estimated by using the following method.

In Fig. 4, O is a point in a conductor foil which intersects the x–y plane with an elevation angle of θ. The temperature gradient at point O along the conductor foil is expressed as:

$$\frac{\partial T}{\partial \xi_\theta} = \cos\theta \frac{\partial T}{\partial y} + \sin\theta \frac{\partial T}{\partial z} \qquad (7)$$

where ξ_θ is the direction pointing toward the tab terminal with an elevation angle of θ to the y axis. The heat flux along the conductor foil, N_θ, is thus expressed as

$$N_\theta = -\varepsilon_c k_c \frac{\partial T}{\partial \xi_\theta} = -\varepsilon_c k_c \left(\cos\theta \frac{\partial T}{\partial y} + \sin\theta \frac{\partial T}{\partial z} \right) \qquad (8)$$

The heat flux in the y and z directions is the components of N_θ in the corresponding directions and are expressed as:

$$N_y = \cos\theta N_\theta = -\varepsilon_c k_c \left(\cos^2\theta \frac{\partial T}{\partial y} + \sin\theta \cos\theta \frac{\partial T}{\partial z} \right) \qquad (9)$$

$$N_z = \sin\theta N_\theta = -\varepsilon_c k_c \left(\sin\theta \cos\theta \frac{\partial T}{\partial y} + \sin^2\theta \frac{\partial T}{\partial z} \right) \qquad (10)$$

As the conductor foils are continuous in the x direction, the heat flux in this direction is expressed as:

$$N_x = -\varepsilon_c k_c \frac{\partial T}{\partial x} \qquad (11)$$

Therefore, the heat flux vector at point O is as follows:

$$\begin{bmatrix} N_x \\ N_y \\ N_z \end{bmatrix} = -\varepsilon_c k_c \begin{bmatrix} 1 & 0 & 0 \\ 0 & \cos^2\theta & \sin\theta\cos\theta \\ 0 & \sin\theta\cos\theta & \sin^2\theta \end{bmatrix} \begin{bmatrix} \dfrac{\partial T}{\partial x} \\ \dfrac{\partial T}{\partial y} \\ \dfrac{\partial T}{\partial z} \end{bmatrix} \qquad (12)$$

Next, define the orientation matrix $\underline{\underline{\Theta}}$ as:

$$\underline{\underline{\Theta}} = \begin{bmatrix} 1 & 0 & 0 \\ 0 & \cos^2\theta & \sin\theta\cos\theta \\ 0 & \sin\theta\cos\theta & \sin^2\theta \end{bmatrix} \qquad (13)$$

and the thermal conductivity matrix of the tab base is obtained as:

$$\underline{\underline{k}} = \varepsilon_c k_c \underline{\underline{\Theta}} \qquad (14)$$

Similarly, the electrical conductivity matrix of the tab base is expressed as:

$$\underline{\underline{\sigma}} = \varepsilon_c \sigma_c \underline{\underline{\Theta}} \qquad (15)$$

The derivation of the expressions for $\sin\theta$ and $\cos\theta$ as functions of location is presented in Appendix A.

The volumetric current source is zero in the tab bases and the volumetric heat source has the same expression as equation (5).

2.3.4. Electroactive regions of the cells

In these domains, the two modified potentials, Φ_L and Φ_R, are both defined; therefore, there are two electrical equations in the electroactive region of each cell and the electrical conductivity takes different values for the two potentials. The values of $\underline{\underline{\sigma}}$ for the two electrical equations in the electroactive regions of different
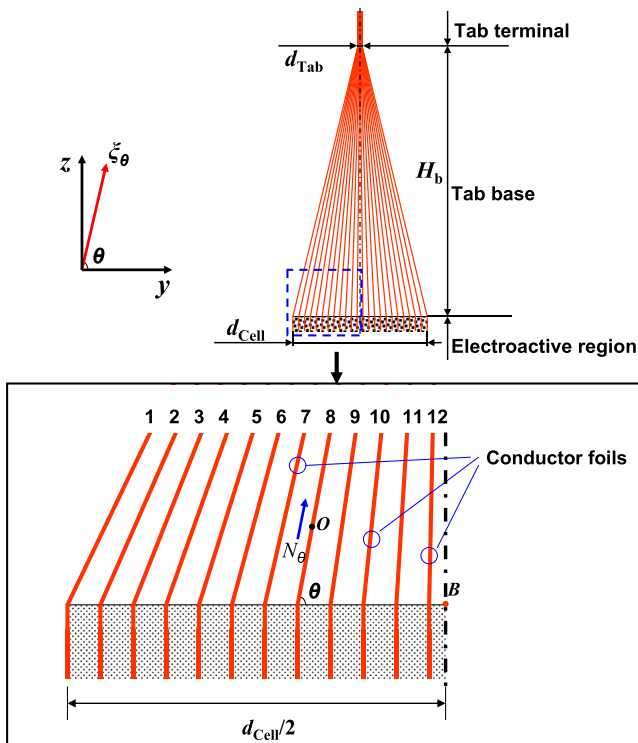
cells are listed in the first two rows of Table 2, where the diagonal orientation matrix is defined as follow:

$$\text{diag}(1,0,1) = \begin{bmatrix} 1 & 0 & 0 \\ 0 & 0 & 0 \\ 0 & 0 & 1 \end{bmatrix} \tag{16}$$

Next, assume that in each cell (see Fig. 5), there are N_d doubled-sided positive electrode plates and $N_d - 1$ doubled-sided negative electrode plates setting in the middle, and 2 single-sided negative electrode plates located at the exterior layers. Therefore, in each cell, there are totally N_d sheets of current collector foils for the positive electrode and $N_d + 1$ sheets for the negative electrode (e.g., $N_d = 24$ for the cell in Ref. [9]) The planar cross-sections of all the electrode active layers are regarded as equal-sized, so the volume fractions of the current collectors of the electrodes in the cell electroactive regions, $\varepsilon_{c,+}$ and $\varepsilon_{c,-}$, are estimated by the following equations:

$$\varepsilon_{c,+} = N_d \frac{A_c d_{c,+}}{V_{\varOmega_E}} \tag{17}$$

$$\varepsilon_{c,-} = (N_d + 1) \frac{A_c d_{c,-}}{V_{\varOmega_E}} \tag{18}$$

where A_c is the planar cross-section area of each electroactive region, $d_{c,+}$ and $d_{c,-}$ are the current collector thicknesses of the positive and negative electrodes, and $V_{\varOmega_E}$ is the volume of the cell electroactive region including the current collectors. By neglecting the volume of cell pouch casing, the value of $V_{\varOmega_E}$ is calculated directly from the cell dimensions shown in Fig. 2.

The expressions for the volumetric current sources in the electroactive regions of different cells are listed in the last two rows of Table 2, where $a_{c,+}$ and $a_{c,-}$ are the specific electroactive surface area for the current collectors of the two electrodes, and i_N is the normal inward current density passing through the electroactive surface of the positive electrode current collector. For the double-sided electrode plates, both sides are electroactive surfaces, while for the single-sided ones, only the one side with an active material coating is electroactive. Therefore, for both the positive and negative electrodes, the total electroactive surface area of current collector is $2N_d A_c$, and $a_{c,+}$ and $a_{c,-}$ are determined as follows:

$$a_{c,+} = a_{c,-} = \frac{2N_d A_c}{V_{\varOmega_E}} \tag{19}$$

The surface current density term, i_N, is a coupling variable returned from the electrochemical sub-model. According to Ref. [19], i_N is approximated by the average current density across the electrode plate pairs:

$$i_N \approx -\frac{I_{app}}{2N_d A_c} \tag{20}$$

where I_{app} is the current applied to the battery module and is defined as positive for charge and negative for discharge. Equation (20) is applied for each of the three cells as the limiting equations

Table 2
Expressions for the electrical conductivities and volumetric current densities in the electroactive regions of different cells.

		Cell 1	Cell 2	Cell 3
$\underline{\underline{\sigma}}$	For $\varPhi_L$	$\varepsilon_{c,-}\sigma_{c,-}\text{diag}(1,0,1)$	$\varepsilon_{c,+}\sigma_{c,+}\text{diag}(1,0,1)$	$\varepsilon_{c,-}\sigma_{c,-}\text{diag}(1,0,1)$
	For $\varPhi_R$	$\varepsilon_{c,+}\sigma_{c,+}\text{diag}(1,0,1)$	$\varepsilon_{c,-}\sigma_{c,-}\text{diag}(1,0,1)$	$\varepsilon_{c,+}\sigma_{c,+}\text{diag}(1,0,1)$
i_v	For $\varPhi_L$	$-a_{c,-}i_N$	$a_{c,+}i_N$	$-a_{c,-}i_N$
	For $\varPhi_R$	$a_{c,+}i_N$	$-a_{c,-}i_N$	$a_{c,+}i_N$

from which the three time-dependent reference potentials, $V_1(t)$, $V_2(t)$, and $V_3(t)$, are determined.

The anisotropic thermal conductivity matrix in the cell electroactive region is expressed as:

$$\underline{\underline{\mathbf{k}}} = \begin{bmatrix} k_{\text{planar}} & 0 & 0 \\ 0 & k_{\text{transv}} & 0 \\ 0 & 0 & k_{\text{planar}} \end{bmatrix} \tag{21}$$

where k_{planar} is the planar thermal conductivity in the x and z directions, and k_{transv} is the transversal thermal conductivity in the y direction. The volumetric heat source in the cell electroactive region is expressed as the sum of the Joule heating rates of the two potentials and the electrochemical heat generated through the electrode coatings and separator:

$$Q_v = \left(-\underline{\underline{\sigma}}\nabla\varPhi_L\right)\cdot\left(-\nabla\varPhi_L\right) + \left(-\underline{\underline{\sigma}}\nabla\varPhi_R\right)\cdot\left(-\nabla\varPhi_R\right) + \varepsilon_e Q_{ECh} \tag{22}$$

where ε_e is the volume fraction of the electrode coatings and separator in the cell electroactive region, and Q_{ECh} is the electrochemical heat source. The expression for ε_e is estimated as:

$$\varepsilon_e = 2N_d \frac{A_c(l_p + l_s + l_n)}{V_{\varOmega_E}} \tag{23}$$

where l_p, l_n, and l_s are the thickness for the positive and negative electrode coatings and separator.

According to Ref. [19], Q_{ECh} can be approximated by the following linear correlation;

$$Q_{ECh} \approx Q_{ECh}\big|_{T^{ave},\varPhi_+^{ave},\varPhi_-^{ave}} + \frac{\partial Q_{ECh}}{\partial \varPhi_+}\bigg|_{T^{ave},\varPhi_+^{ave},\varPhi_-^{ave}}\left(\varPhi_+ - \varPhi_+^{ave}\right) + \frac{\partial Q_{ECh}}{\partial \varPhi_-}\bigg|_{T^{ave},\varPhi_+^{ave},\varPhi_-^{ave}}\left(\varPhi_- - \varPhi_-^{ave}\right) \tag{24}$$

where T, $\varPhi_+$, and $\varPhi_-$ are the volume-average temperature and potentials in the electroactive region of each cell, and the terms $Q_{ECh}\big|_{T^{ave},\varPhi_+^{ave},\varPhi_-^{ave}}$, $(\partial Q_{ECh}/\partial \varPhi_+)\big|_{T^{ave},\varPhi_+^{ave},\varPhi_-^{ave}}$ and $(\partial Q_{ECh}/\partial \varPhi_-)_{T^{ave},\varPhi_+^{ave},\varPhi_-^{ave}}$ are the output variables and their derivatives of the electrochemical sub-model evaluated at the volume-average temperature and potentials. The volume-average temperature and potentials are expressed as:

$$T^{ave} = \frac{1}{V_{\varOmega_E}} \iiint_{\varOmega_E} T dv \tag{25}$$

$$\varPhi_+^{ave} = \frac{1}{V_{\varOmega_E}} \iiint_{\varOmega_E} \varPhi_+ dv \tag{26}$$

$$\varPhi_-^{ave} = \frac{1}{V_{\varOmega_E}} \iiint_{\varOmega_E} \varPhi_- dv \tag{27}$$

where $\varOmega_E$ is domain symbol for the cell electroactive domain.

2.4. Electrical and thermal boundary conditions

In a discharge process, the applied current, I_{app}, is set to enter the battery module from the negative electrode tab terminal of cell 1 and exit through the positive electrode tab terminal of cell 3; and the inlet and outlet electrical boundary conditions are, respectively, expressed as:
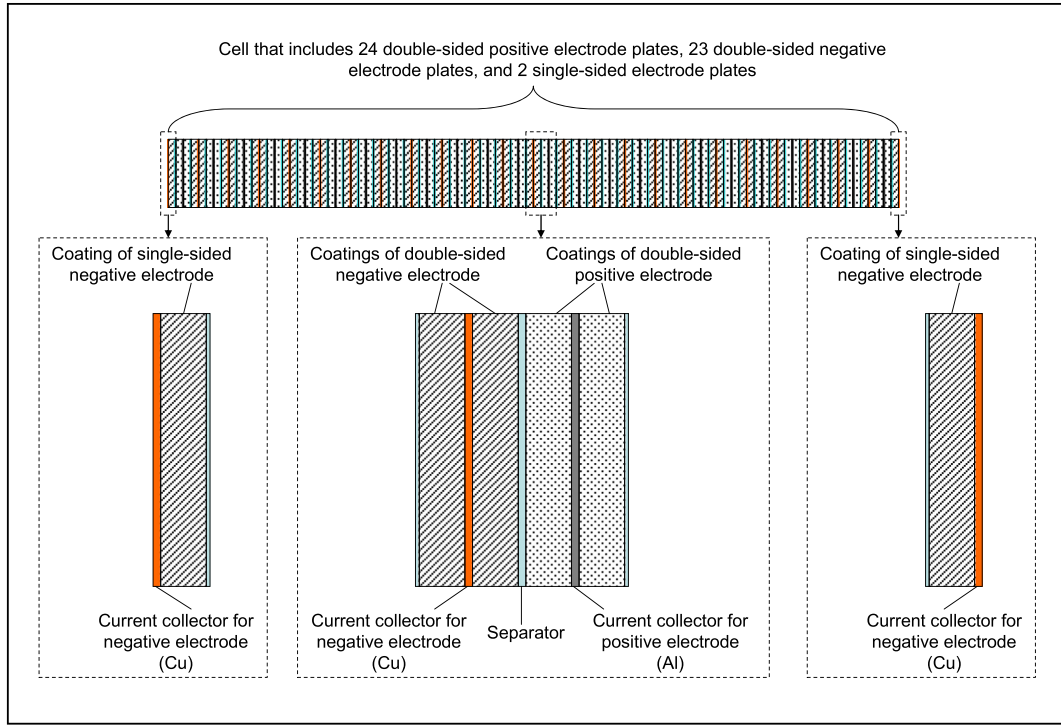
(a) Arrangement of electrode plates in one cell
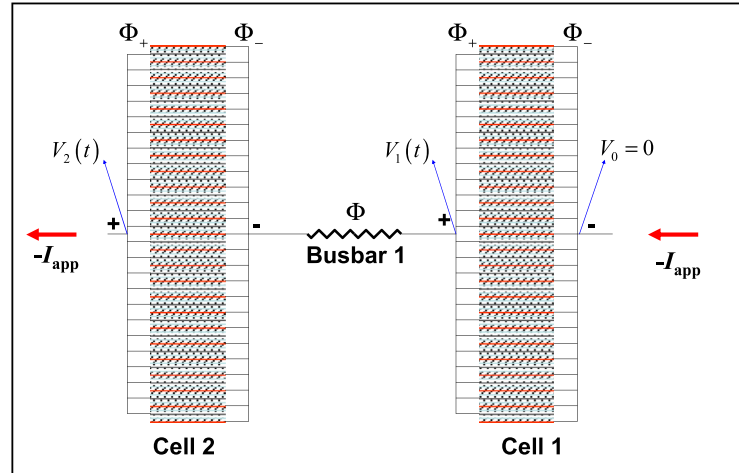
(b) Connection of electrode plates in cell 1 and 2 through busbar

Fig. 5. Configuration of a cell that includes 24 double-sided positive electrode plates, 23 double-sided negative electrode plates, and 2 single-sided negative electrode plates.

$$\text{Inlet}: \quad n \cdot \left(-\underline{\underline{\boldsymbol{\sigma}}} \, \nabla \varPhi_{\mathrm{L}} \right) \; = \frac{I_{\mathrm{app}}}{A_{\partial \varOmega}} \tag{28}$$

$$\text{Outlet}: \quad n \cdot \left(-\underline{\underline{\boldsymbol{\sigma}}} \, \nabla \varPhi_{\mathrm{R}} \right) \; = -\frac{I_{\mathrm{app}}}{A_{\partial \varOmega}} \tag{29}$$

where n is the normal unit vector pointing out of the boundary, and $A_{\partial \varOmega}$ is the area of the boundary surface. All the other exterior surfaces of the battery module are set as electrical insulation.

In this model, the thermal boundary conditions on the battery module surfaces are subject to Newton's law of heat transfer. Weak convection is assumed in the spaces between the two neighboring cell surfaces, and the boundary heat flux depends on the temperature difference between the two opposite cell surfaces. For example, the left boundary of cell 2 (with temperature $T_{2,\mathrm{L}}$) directly faces the right boundary of cell 1 (with temperature $T_{1,\mathrm{R}}$), and thus the outward surface heat flux from the left boundary of cell 2 is expressed as:

$$n \cdot \left(-\underline{\underline{\mathbf{k}}} \, \nabla T \right) \; = h_{\mathrm{c,in}} \left(T_{2,\mathrm{L}} - T_{1,\mathrm{R}} \right) \tag{30}$$

where $h_{\mathrm{c,in}}$ is the convective heat transfer coefficient in the spaces between the two neighboring cell surfaces. For the other surfaces that are exposed to the outer environment, the outward surface heat flux from these boundaries are expressed as:

Table 3
Parameter values for the electrical and thermal equations.

Region	Parameter	Value
Electroactive region of cell	Rate capacity of cell C (Ah)	20
	Specific heat capacity C_p (J kg^{-1} K^{-1})	572
	Thickness of positive electrode current collector $d_{c,+}$ (m)	10×10^{-6}
	Thickness of negative electrode current collector $d_{c,-}$ (m)	15×10^{-6}
	Thickness of cell d_{cell} (m)	9×10^{-3}
	Heat transfer coefficient between surface and outer environments $h_{c,ext}$ (W m^{-2} K^{-1})	15
	Heat transfer coefficient between neighboring cell surfaces $h_{c,in}$ (W m^{-2} K^{-1})	0.28
	Planar thermal conductivity k_{planar} (W m^{-1} K^{-1})	27
	Transversal thermal conductivity k_{transv} (W m^{-1} K^{-1})	0.8
	Number of double-sided positive electrode plates N_d	24
	Density of domain material ρ (kg m^{-3})	4500
	Electrical conductivity for positive electrode $\sigma_{c,+}$ (S m^{-1})	37.8×10^6
	Electrical conductivity for negative electrode $\sigma_{c,-}$ (S m^{-1})	59.6×10^6
Tab base of positive electrode	Specific heat capacity C_p (J kg^{-1} K^{-1})	896
	Thermal conductivity k_c (W m^{-1} K^{-1})	237
	Density of conductors ρ_c (kg m^{-3})	2700
	Electrical conductivity σ_c (S m^{-1})	37.8×10^6
Tab base of negative electrode	Specific heat capacity C_p (J kg^{-1} K^{-1})	383
	Thermal conductivity k_c (W m^{-1} K^{-1})	401
	Density of conductors ρ_c (kg m^{-3})	8900
	Electrical conductivity σ_c (S m^{-1})	59.6×10^6
Tab terminal of positive electrode	Specific heat capacity C_p (J kg^{-1} K^{-1})	896
	Thermal conductivity k_c (W m^{-1} K^{-1})	237
	Density of domain material ρ (kg m^{-3})	2700
	Electrical conductivity σ_c (S m^{-1})	37.8×10^6
Tab terminal of negative electrode	Specific heat capacity C_p (J kg^{-1} K^{-1})	383
	Thermal conductivity k_c (W m^{-1} K^{-1})	401
	Density of domain material ρ (kg m^{-3})	8900
	Electrical conductivity σ_c (S m^{-1})	59.6×10^6
Busbar	Specific heat capacity C_p (J kg^{-1} K^{-1})	383
	Thermal conductivity k_c (W m^{-1} K^{-1})	401
	Density of domain material ρ (kg m^{-3})	8900
	Electrical conductivity σ_c (S m^{-1})	59.6×10^6

$$n \cdot \left(-\underline{\underline{\mathbf{k}}} \nabla T \right) = h_{c,ext}(T - T_{amb}) \tag{31}$$

where $h_{c,ext}$ is the heat transfer coefficient between the cell surface and the outer environments, and T_{amb} is the ambient temperature.

2.5. Electrochemical sub-model

The electrochemical sub-model in a multi-scale framework is usually described as a block which receives the temperature and current collector potentials as input and provides the transversal current density and electrochemical heat generation as output [19]. Several reported models can be incorporated for this purpose, i.e. the empirical model by Newman and Tiedeman [6,20], the state-variable model by Smith et al. [11], or the equivalent circuit model by Chen et al. [21]. In this work, Newman's pseudo-2D (P2D) model is chosen as the electrochemical sub-model to describe the transport phenomena and interface reaction kinetics through the electrode coatings and separator of the Li-ion cell. To avoid a huge computation load, the linear approximation approach presented in Ref. [19] was employed to simply the model coupling. Therefore, only one P2D model is attached to each cell. The details for the P2D model are presented in Appendix B.

2.6. Model input

The values for the parameters in the electrical and thermal equations are listed in Table 3. Parameter values for the electrochemical sub-model are obtained from Ref. [19] and presented in Appendix B. The electrical and thermal boundary conditions are customizable inputs which enable this model to be integrated into more complicated system models. For example, if thermal management is considered, this model can be linked to the CFD/thermal models of cooling devices through the boundary heat flux at the cell surfaces. Since transient CFD simulations are expensive, we just apply constant heat transfer coefficients for our case studies.

3. Results and discussion

With the mathematical model presented above, discharge processes at 1 C, 3 C, and 5 C were simulated, where the end-of-discharge condition is set as $V_3(t) = 9.0$ V. The simulations take about 30 s with 2.6 G computer memory in a PC. The simulated

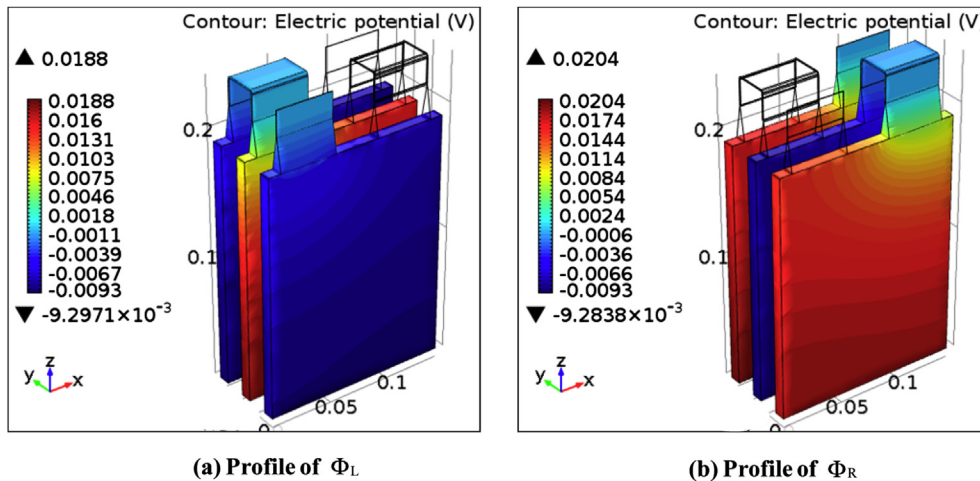**(a) Profile of Φ_L**

(b) Profile of Φ_R

Fig. 6. Profiles of modified potentials across the module at the end of 5 C discharge.
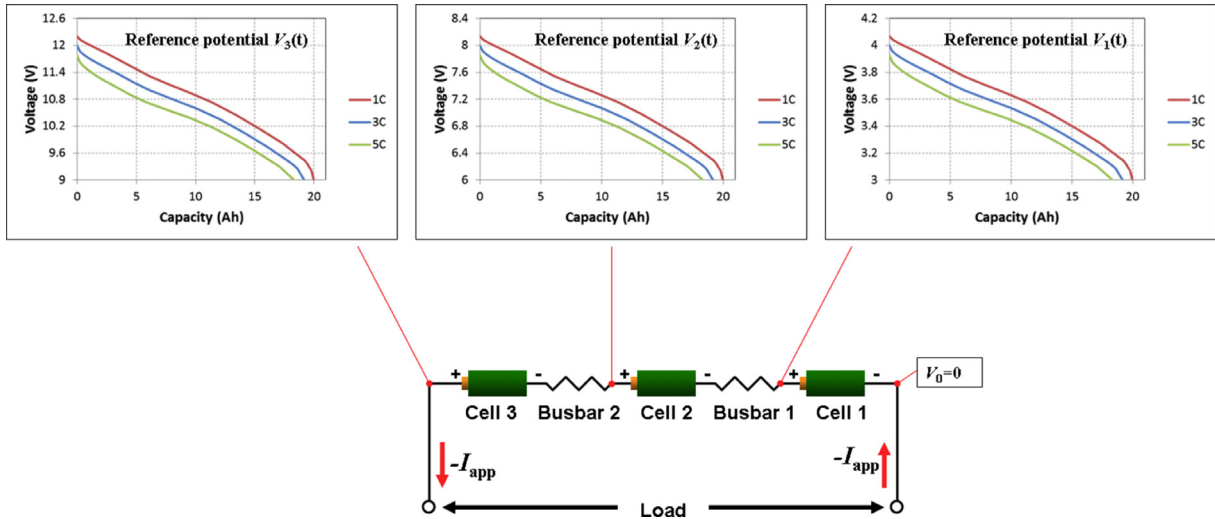
Fig. 7. Plots for the reference potentials vs.

electrical, thermal, and electrochemical behavior of the battery module are presented in the following sections.

3.1. Electrical results

The profiles for the two modified potentials through the entire battery module at the end of 5 C discharge (where $t = 684$ s) are presented in Fig. 6. The plots for the three time-dependent reference potentials at 1 C, 3 C, and 5 C are presented in Fig. 7, in which a circuit diagram shows symbolically the location of each reference potential. The profiles for the actual current collector potentials of the two electrodes in cell 2 (the cell in the middle) at the end of 5 C discharge are presented in Fig. 8. The profiles for the modified potentials through the module at the end of 1 C and 3 C discharge processes are presented in Fig. 9.

As shown in Fig. 8, the potential of each electrode rises or drops more steeply near the tab base than at other locations. The reason is that the two tab bases, which have very small effective cross-section area (the effective cross-section area of tab base is the actual geometric cross-section area scaled by the conductor volume fraction ε_c), act as bottlenecks to the conductive current flow to enter or exit the cell electroactive region; and therefore, the high conductive current density near the tab bases generates large local potential gradients. Comparing the individual potential profiles for the two electrodes, the positive electrode has a larger potential gradient than the negative electrode, and the reason for this difference is that the current collector for the positive electrode (aluminum) has a smaller electrical conductivity than that for the negative electrode (copper). According to Fig. 9, the electrical potential profiles are more uniform at lower current rates.

The potential profiles for the positive electrode tab base of cell 1 and busbar 1 at the end of 5 C discharge are shown in Fig. 10(a) and (b), where the black arrows denote the directions for the conductive current flow, the length of each arrow is proportional to the norm value of the local current density. As shown in the left plot, the conductive current flows radially toward the tab terminal, and the magnitude of conductive current density is larger at higher locations than at lower locations. According to equation (15), the electrical conductivity of the tab base is proportional to the conductor foil volume fraction ε_c; and the value of ε_c increases (see Fig. A2) as the space between the foils drop with the height of location; therefore, the norm of conductive current density gets larger in accordance with the increasing electrical conductivity from the bottom to the top of the tab base. In this work, copper is chosen as the busbar material; and as shown in the right plot, due to large electrical conductivity, the potential drop through the
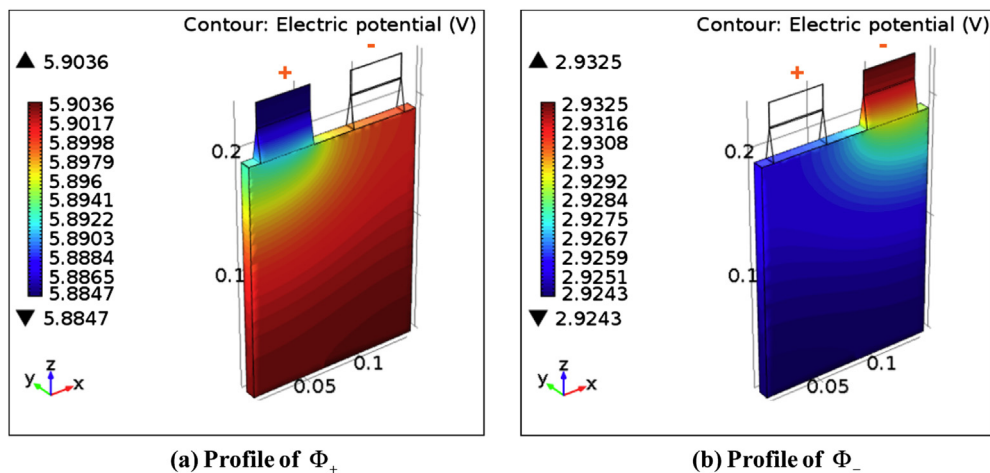

(a) Profile of Φ_+

(b) Profile of Φ_-

Fig. 8. Profiles of positive and negative electrode potentials of cell 2 at the end of 5 C discharge.

(a) Φ_L profile at the end of 1C discharge

(b) Φ_L profile at the end of 3C discharge

(c) Φ_R profile at the end of 1C discharge

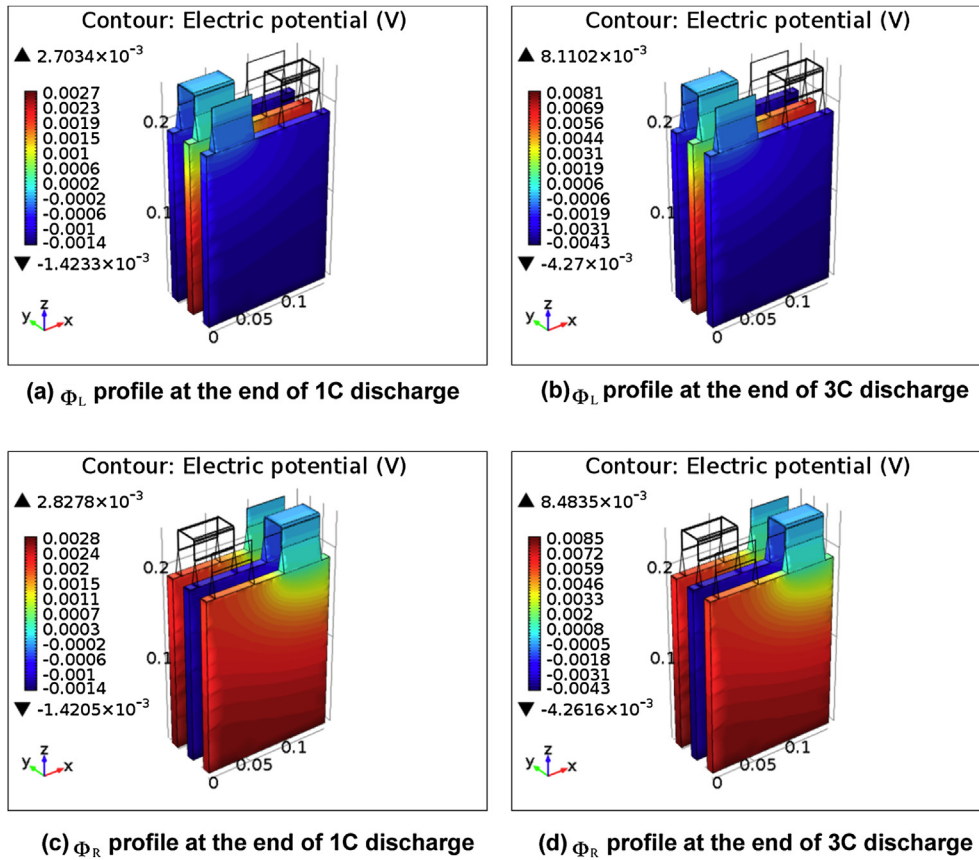(d) Φ_R profile at the end of 3C discharge

Fig. 9. The profiles of modified potentials at the end of 1 C and 3 C discharge processes.

busbar is very small (only 2 mV). The magnitude of conductive current density is uniformly distributed through the busbar domain because the electrical conductivity is isotropic in the busbar.

3.2. Thermal results

The temperature profiles through the entire 3S module and the individual cells at the end of 5 C discharge are presented in Fig. 11. As shown in these plots, cell 2, which is located in the middle of the 3S module, is hotter than the other two cells by about 2°. The

reason is that both sides of cell 2 are exposed to the weak convection spaces; while the other two cells have only one side exposed to the weak convection and another side to the outer environment with higher convective heat transfer rates. In each cell, regions near the positive electrode tab bases have higher temperature than other locations; the reasons for this include the high current density near the tab bases and the low electrical conductivity of the positive electrode current collector. The end-of-discharge temperature profiles for 1 C and 3 C processes are presented in Fig. 12, and according to these thermal plots, the position
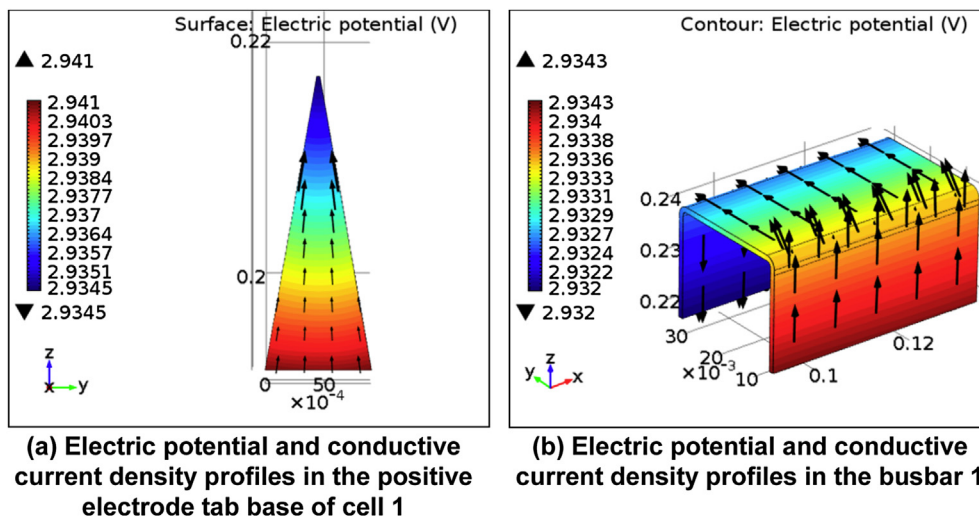

(a) Electric potential and conductive current density profiles in the positive electrode tab base of cell 1

(b) Electric potential and conductive current density profiles in the busbar 1

Fig. 10. Electric potential and conductive current profiles in the positive electrode tab base of cell 1 (a) and in busbar 1.
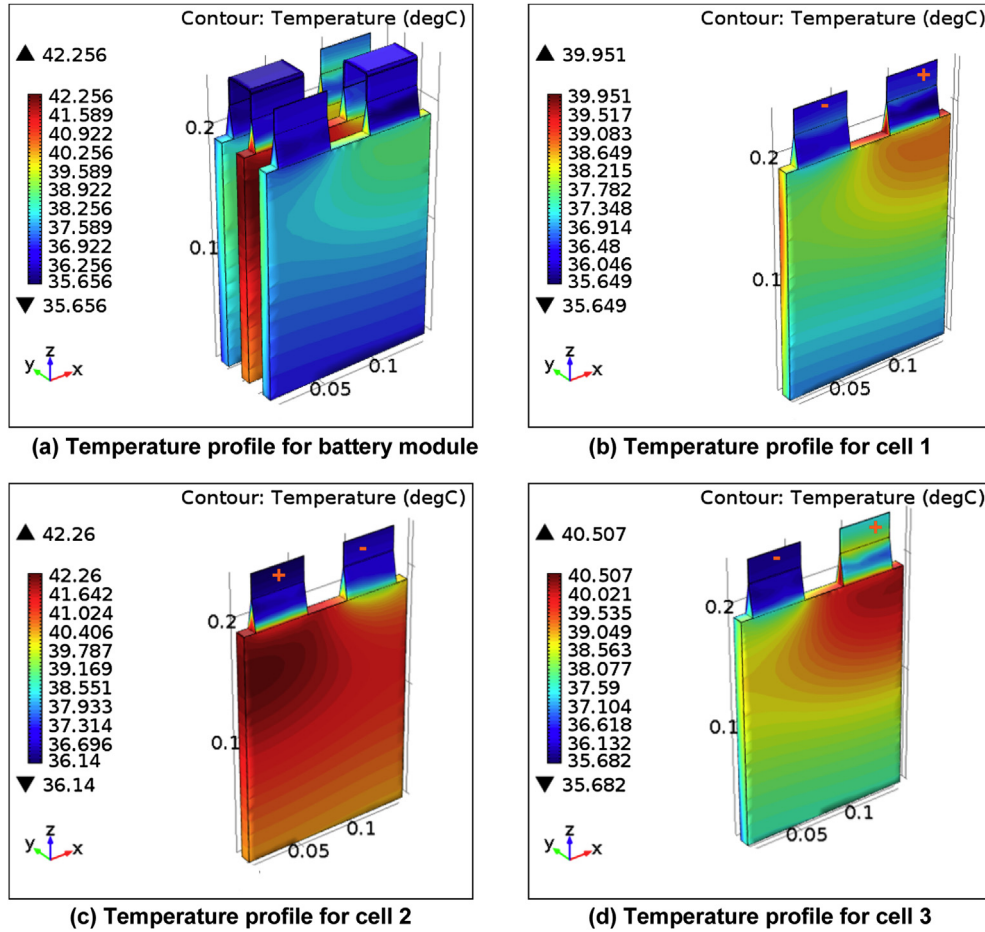
Fig. 11. Profiles of temperature across the module and for individual cells at the end of 5 C discharge.

of the hot spot in each cell gets lower as the current rate decreases, and this phenomenon can be explained by the temperature vs time plots in Fig. 13. The temperature difference between the electro-active region and the two tabs increases with time, therefore, as a result of the increasing temperature gradient from the bottom to the top of a cell, the hot spot in a cell moves downward during the discharge. Due to the longer discharge time, the hot spot goes to a lower position at low current rates than at higher rates.

The thermal plots for the positive electrode tab base of cell 2 and busbar 2 at the end of 5 C discharge are presented separately in Fig. 14. As shown in Fig. 14(a), the lower parts of the tab base are hotter than the higher parts because the anisotropic thermal conductivity of the tab base increases with height (same reason as the electrical conductivity variation). At the same height, the center region of the tab base is hotter than the exterior parts, the reason for this is that the conductor foils arrayed near the center plane of
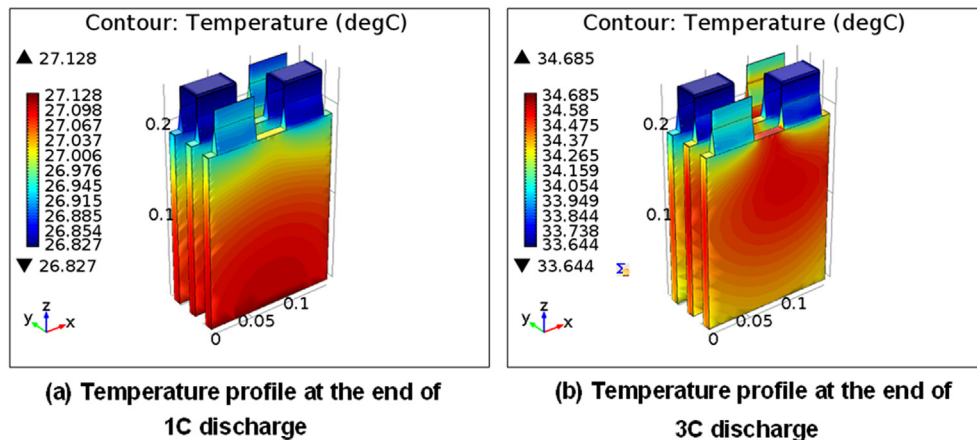

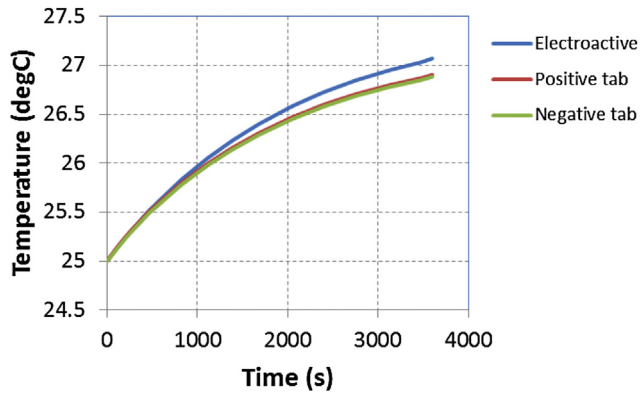**Fig. 12.** Temperature profiles at the end of 1 C and 3 C discharge processes.

Fig. 13. The volume-average temperature of different regions in cell 2 during 1 C discharge.

the tab base have elevation angles close to 90° (see Fig. A2), and the heat flux in the *y* direction, which is scaled by cos θ according to equation (9), is very small. The temperature of the exterior surfaces of the tab base is much lower than the center due to the high external heat transfer rates. As presented in Fig. 14(b), the temperature of busbar is lower than that of the tab base and changes by only 0.4 °C through the domain, because the busbar is thin and has a large isotropic thermal conductivity which allows the heat to be

dissipated to the surroundings easily and make the temperature gradients small. The profile of the Joule heating rate in busbar 2 is presented in Fig. 14(c) where it can be seen that the heat source is uniformly distributed throughout the busbar in accordance with the uniform distribution of conductive current flow as presented in Fig. 10(b).

3.3. Electrochemical results

According to the equations listed in Table B1, the transport and kinetic processes of P2D electrochemical sub-model are affected by the temperature input. As stated previously, the P2D sub-model is called at the volume-average temperature in the electroactive region of the individual cell to which the P2D sub-model is attached. The three cells have different temperatures, and the electrochemical behavior of these cells varies accordingly. As shown in Fig. 15(a), the average-temperature of cell 2 is higher than those of cell 1 and 3; therefore, as shown in Fig. 15(b), the electrolyte potential drop through the porous electrode regions of cell 2 is slightly smaller than those of the other two cells because the ion conductivity of electrolyte increases with temperature. As presented in Fig. 15(c), the electrochemical heat generation rate in cell 2 is slightly smaller than those in the other two cells, due to the higher ion conductivity in the electrolyte and the smaller mass transfer resistivity in both the solid and solution phases and the smaller charge transfer resistivity for the electrochemical reactions.
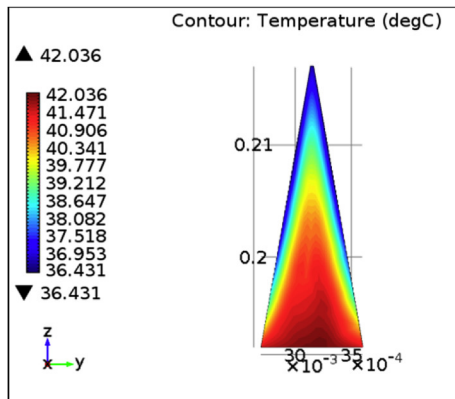
(a) Temperature profile for the positive electrode tab base of cell 2
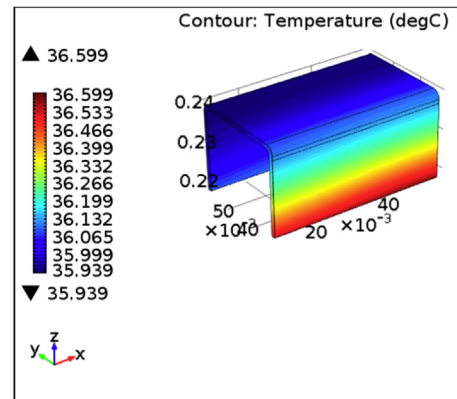
(b) Temperature profile for busbar 2
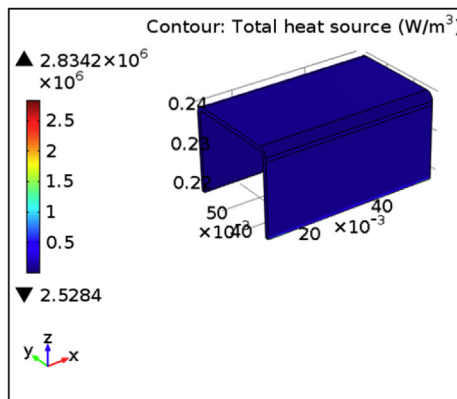
(c) Heat source profile for busbar 2

Fig. 14. Profiles for the temperature in the positive electrode tab base of cell 2 (a) and busbar 2 (b), and the total heat source in the busbar 2 (c) at the end of 5 C discharge.
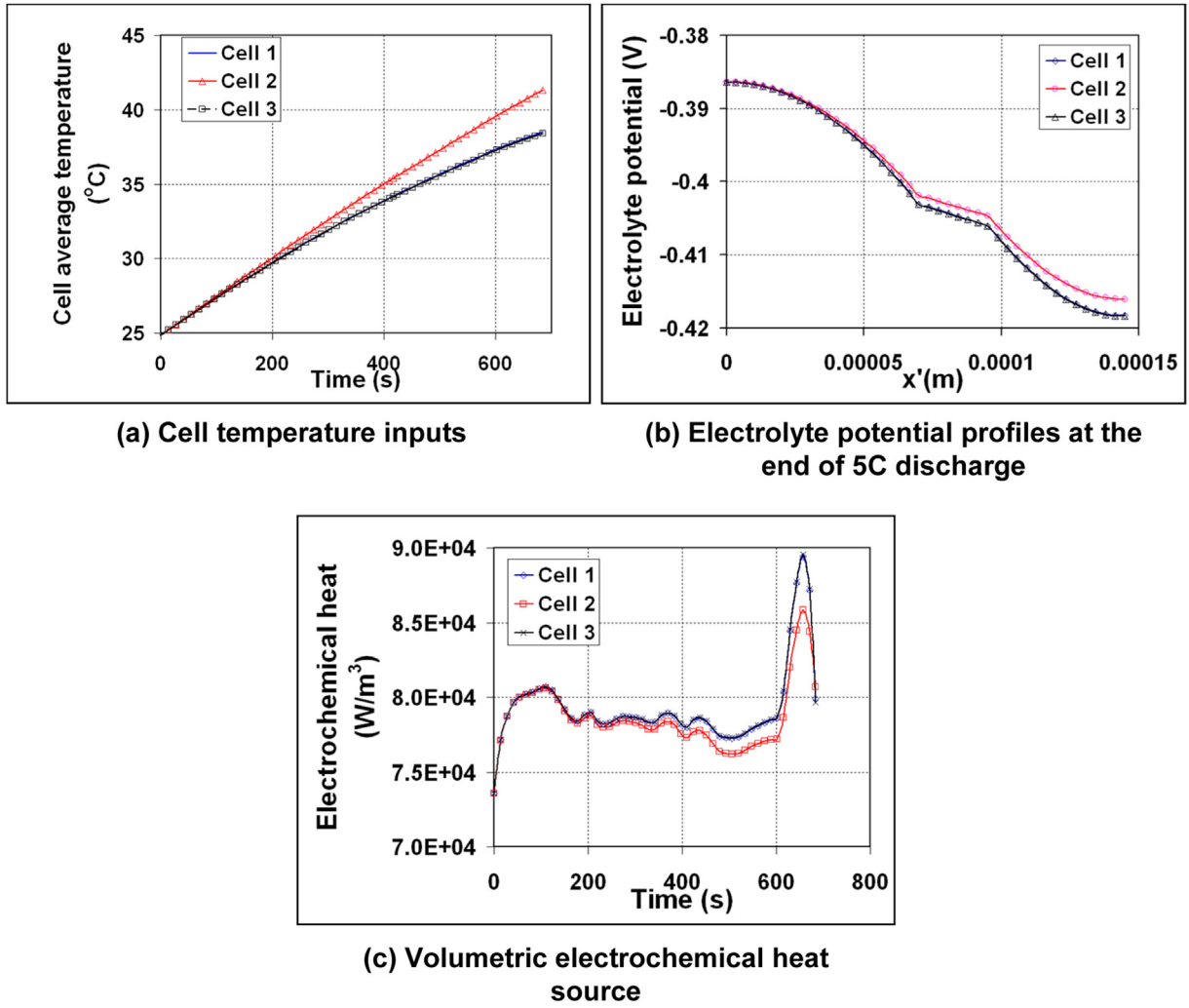
(a) Cell temperature inputs

(b) Electrolyte potential profiles at the end of 5C discharge

(c) Volumetric electrochemical heat source

Fig. 15. The temperature-dependent electrochemical behaviors of cells during 5 C discharge.

4. Conclusion

In this work, a standardized 3D multi-physics model template for a Li-ion battery was developed to predict the distributed electrical and thermal behavior of the cells and connectors. By using a simplified model-coupling approach, the computational load for this model is low and the simulation takes less than 1 min on a PC. This model may be useful in the design of a battery configuration. The model template also has very good extendibility; it can be easily coupled with other multi-physics equations to implement system analysis, or be embedded into control software. Since the goal for our research work for this first step has been achieved; in the next step, we will shift our focus from the model development to the extended applications of this model, i.e. the validation of this model with experimental data, the inclusion of more cells with complex parallel-series configurations, and the integration of a cooling system.

Appendix A

According to Fig. 4, the left-half of the tab base cross-section in the $y-z$ plane can be regarded as a trapezoid, and the geometry details are shown in Fig. A1, where trapezoid $ABCD$ denotes the left-half of the tab base cross-section, d_{Cell} denotes the thickness of the electroactive region, d_{Tab} denotes the thickness of the tab terminal, and B is the midpoint of the bottom facet of the tab base. Point O is located at the intersection between a specific conductor foil plane and the $y-z$ plane, and θ is the angle of elevation for the conductor foil plane. The distances of point O to the segments $|AB|$ and $|BC|$ are expressed as:

$$|OG| = y_B - y_O \tag{A-32}$$

$$|BG| = z_O - z_B \tag{A-33}$$

where y_O, z_O, y_B, and z_B are the coordinates of points O and B.

Assuming that the conductor foils are arrayed with equal displacements at the same height, the following proportional relationship is obtained as:

$$\frac{|OG|}{|FG|} = \frac{|BE|}{|AB|} \tag{A-34}$$

while other geometry relationships include:

$$\text{Area of Trapezoid } ABGF: \varLambda_{ABGF} = \frac{1}{2}(|AB| + |FG|)|BG| \tag{A-35}$$

Area of Trapezoid $CDFG$: $\Lambda_{CDFG} = \frac{1}{2}(|FG| + |CD|)|CG|$ (A-36)

Area of Trapezoid $ABCD$: $\Lambda_{ABCD} = \frac{1}{2}(|AB| + |CD|)|BC|$ (A-37)

$$\Lambda_{ABCD} = \Lambda_{ABGF} + \Lambda_{CDGF} \tag{A-38}$$

where

$$|AB| = \frac{d_{Cell}}{2} \tag{A-39}$$

$$|CD| = \frac{d_{Tab}}{2} \tag{A-40}$$

$$|BC| = H_b \tag{A-41}$$

It can be obtained from equations (A-34)–(A-38) that the length of segment $|BE|$ is expressed as:

$$|BE| = \frac{d_{Cell}H_b(y_B - y_O)}{d_{Cell}H_b - (d_{Cell} - d_{Tab})(z_O - z_B)} \tag{A-42}$$

Therefore, it is obtained that:

$$\cos\theta = \frac{|BE| - |OG|}{\sqrt{(|BE| - |OG|)^2 + |BG|^2}}$$

$$= \frac{(d_{Cell} - d_{Tab})(y_B - y_O)}{\sqrt{[(d_{Cell} - d_{Tab})(y_B - y_O)]^2 + [d_{Cell}H_b - (d_{Cell} - d_{Tab})(z_O - z_B)]^2}} \tag{A-43}$$

$$\sin\theta = \frac{|BG|}{\sqrt{(|BE| - |OG|)^2 + |BG|^2}}$$

$$= \frac{d_{Cell}H_b - (d_{Cell} - d_{Tab})(z_O - z_B)}{\sqrt{[(d_{Cell} - d_{Tab})(y_B - y_O)]^2 + [d_{Cell}H_b - (d_{Cell} - d_{Tab})(z_O - z_B)]^2}} \tag{A-44}$$

Equations (A-43) and (A-44) suggest that the values of $\cos\theta$ and $\sin\theta$ at a specific point in the tab base only depend on the coordinates of that point and the dimensions of the tab base.

Let D_{cc} stands for the total thickness of all the conductor foils in the tab base, therefore, for positive electrode,

$$D_{cc} = N_c d_{c,+} \tag{A-45}$$

and for negative electrode,

$$D_{cc} = (N_c + 1)d_{c,-} \tag{A-46}$$

In the tab base, the volume fraction of conductor, ε_c, is a linear function of $z_O - z_B$. At the bottom of the tab base ($z_O - z_B = 0$),

$$\varepsilon_c = \frac{D_{cc}}{d_{Cell}} \tag{A-47}$$

and at the top of tab base ($z_O - z_B = H_b$),

$$\varepsilon_c = \frac{D_{cc}}{d_{Tab}} \tag{A-48}$$

Therefore, the linear relationship between ε_c and $z_O - z_B \cdot h$ can be obtained from equations (A-47) and (A-48):

$$\varepsilon_c = \left(\frac{D_{cc}}{d_{Tab}} - \frac{D_{cc}}{d_{Cell}}\right)\frac{z_O - z_B}{H_b} + \frac{D_{cc}}{d_{Cell}} \tag{A-49}$$

Therefore, the value of ε_c at a specific point depends only on the height of that point and tab base dimensions.

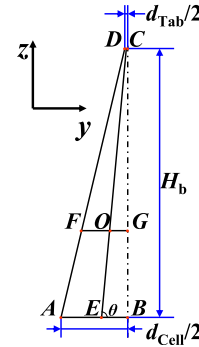The 2D plots for $\cos\theta$, $\sin\theta$, and ε_c in the tab base are presented in Fig. A2.

Fig. A1. Geometry description for the left-half of the tab base cross-section.

(a) Distribution of $\sin\theta$ **(b) Distribution of $\cos\theta$**   **(c) Distribution of ε_c**
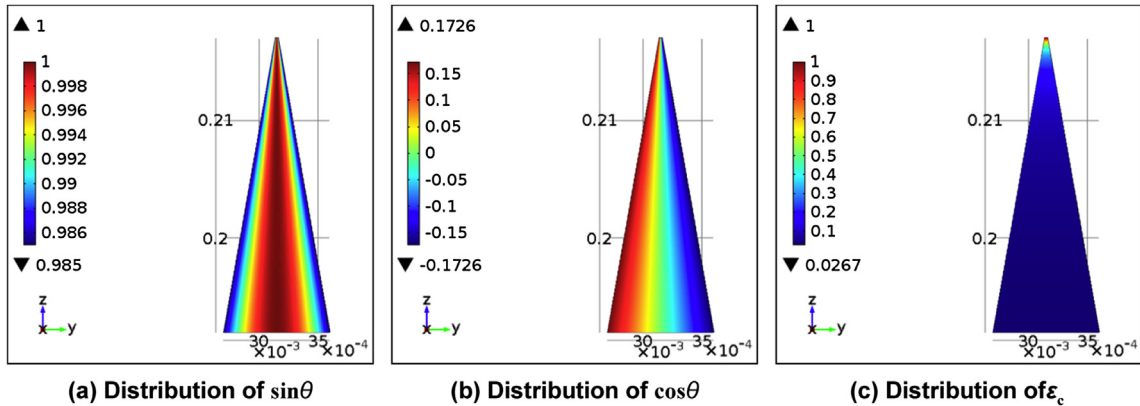
Fig. A2. The sine\cosine functions for the elevation angle and the volume fraction of conductor foils in the tab base.

Appendix B

The Newman's pseudo-2D (P2D) model [16–18] was developed in a porous electrode geometry. Several transport phenomena and kinetic processes are included in the P2D model, and the governing equations are listed in Table B1. In the multi-scale modeling, the input variables of P2D model are temperature and the current collector potentials from the macroscopic models, and the output variables of P2D model are the current density into current collector and the electrochemical heat source. The descriptions of P2D model variables are listed in Table B2, and the parameter values are listed in Table B3.

Table B1
Governing equations for the P2D model.

Model	Equations
Variable inputs	T (Affecting the temperature – dependent transport properties)
	Φ_+ Φ_- (Acting as boundary values for solid phase charge balance)
Solution phase diffusion	$\varepsilon \frac{\partial c_e}{\partial t} = \frac{\partial}{\partial x'}\left(D_{2,\text{eff}}\frac{\partial c_e}{\partial x'}\right) + a(1-t^+)J$ $D_{2,\text{eff}} = D_{e,\text{bulk}}\varepsilon^\beta$ $\frac{\partial c_e}{\partial x'}\big|_{x'=0} = 0$ $\frac{\partial c_e}{\partial x'}\big|_{x'=l_p+l_s+l_n} = 0$
	The source term $a(1-t^+)J$ is neglected in the separator region$(l_p < x' < l_p + l_s)$
	Diffusion coefficient in bulk solusion(m^2/s) :
	$D_{e,\text{bulk}} = 5.84 \times 10^{-7} \exp\left(-2870\frac{1}{T}\right)\left(\frac{c_e}{1000}\right)^2 - 33.9 \times 10^{-7} \exp\left(-2920\frac{1}{T}\right)\left(\frac{c_e}{1000}\right) + 129 \times 10^{-7} \exp\left(-3200\frac{1}{T}\right)$
	Transference number of solution phase :
	$t^+ = 2.67 \times 10^{-4} \exp\left(833\frac{1}{T}\right)\left(\frac{c_e}{1000}\right)^2 + 3.09 \times 10^{-3} \exp\left(653\frac{1}{T}\right)\left(\frac{c_e}{1000}\right) + 0.517 \exp\left(-49.6\frac{1}{T}\right)$
Solution phase charge balance	$\frac{\partial i_2}{\partial x} = aFJ$ $i_2 = -\kappa_{\text{eff}}\frac{\partial \phi_2}{\partial x'} - \frac{2RT}{F}(1-t^+)\left(1+\frac{\text{dln} f_\pm}{\text{dln} c_e}\right)\frac{\partial \ln c_e}{\partial x'}$ $\kappa_{\text{eff}} = \kappa_{\text{bulk}}\varepsilon^\beta$ $i_2|_{x'=0} = 0$ $i_2|_{x'=l_p+l_s+l_n} = 0$
	The source term aFJ is neglected in the separator region$(l_p < x' < l_p + l_s)$
	The electrical conductivity in the bulk solution(S/m) :
	$\kappa_{\text{bulk}} = 3.45 \exp\left(-798\frac{1}{T}\right)\left(\frac{c_e}{1000}\right)^3 - 48.5 \exp\left(-1080\frac{1}{T}\right)\left(\frac{c_e}{1000}\right)^2 + 244 \exp\left(-1440\frac{1}{T}\right)\left(\frac{c_e}{1000}\right)$
Solid phase charge balance	$\frac{\partial i_1}{\partial x'} = -aFJ$ $i_1 = -\sigma_{\text{eff}}\frac{\partial \phi_1}{\partial x'}$ $\sigma_{\text{eff}} = \sigma\varepsilon_s^\beta$ $\phi_1|_{x'=0} = \Phi_+$ $i_1|_{x'=l_p} = 0$ $i_2|_{x'=l_p+l_s} = 0$ $\phi_1|_{x'=l_p+l_s+l_n} = \Phi_-$
	Not applied in the separator region$(l_p < x' < l_p + l_s)$
Butler–Volmer equation for electrochemical reactions	$J = k_r c_e^{0.5}(c_{s,\text{max}} - c_{s,r=R_s})^{0.5} c_{s,r=R_s}^{0.5}\left[\exp\left(\frac{0.5F}{RT}\eta\right) - \exp\left(-\frac{0.5F}{RT}\eta\right)\right]$ $k_r = k_{r,\text{ref}}\exp\left[-\frac{\text{Ea}_{re}}{R}\left(\frac{1}{T} - \frac{1}{T_{\text{ref}}}\right)\right]$
	$\eta = \phi_1 - \phi_2 - U$ $U = U_{\text{ref}} + \frac{\partial U}{\partial T}(T - T_{\text{ref}})$
	Not applied in the separator region$(l_p < x < l_p + l_s)$
	Open circuit potential for positive electrode at reference temperature(V):
	$U_{\text{ref}} = 1.638\theta^{10} - 2.222\theta^9 + 15.056\theta^8 - 23.488\theta^7 + 81.246\theta^6 - 344.566\theta^5 + 621.3475\theta^4 - 554.774\theta^3 + 264.427\theta^2 - 66.3691\theta$
	$+ 11.8058 - 0.61386\exp(5.8201\theta^{136.4})$ (V)
	Open circuit potential for negative electrode at reference temperature (V):
	$U_{\text{ref}} = 0.124 + 1.5\exp(-70\theta) - 0.0351\tan h(12.0482\theta - 3.4458) - 0.0045\tan h(8.4034\theta - 7.5630) - 0.035\tan h$
	$(200\theta - 19.80) - 0.0147\tan h(29.4118\theta - 14.7059) - 0.102\tan h(7.0423\theta - 1.3662) - 0.022\tan h(60.9756\theta_n - 59.7561)$
	$-0.011\tan h(44.2478\theta - 5.4867) - 0.0155\tan h(34.4828\theta - 3.6207)$
	Reaction entropy term $\frac{\partial U}{\partial T}$ is neglected according to reference
Solid phase diffusion	$\frac{\partial c_s}{\partial t} = D_s\frac{1}{r^2}\frac{\partial}{\partial r}\left(r^2\frac{\partial c_s}{\partial r}\right)$ $D_s = D_{s,\text{ref}}\exp\left[-\frac{\text{Ea}_{di}}{R}\left(\frac{1}{T} - \frac{1}{T_{\text{ref}}}\right)\right]$ $-D_s\frac{\partial c_s}{\partial r}\big|_{r=0} = 0$ $-D_s\frac{\partial c_s}{\partial r}\big|_{r=R_s} = J$ $\theta = \frac{c_{s,r=R_s}}{c_{s,\text{max}}}$
	Not applied in the separator region $(l_p < x' < l_p + l_s)$
Variable outputs	$i_N = -i_1|_{x'=0}$ $Q_{\text{ECh}}|_{T,\Phi_+,\Phi_-} = \frac{-i_N(\Phi_+ - \Phi_-) + \int_0^{l_p+l_s+l_n} aFJ\left(T_{\text{ref}}\frac{\partial U}{\partial T} - U_{\text{ref}}\right)dx'}{L_p + L_s + L_n}$ $\frac{\partial Q_{\text{ECh}}}{\partial \Phi_+}\big|_{T,\Phi_+,\Phi_-} \approx -\frac{i_N}{L_p + L_s + L_n}$ $\frac{\partial Q_{\text{ECh}}}{\partial \Phi_-}\big|_{T,\Phi_+,\Phi_-} \approx \frac{i_N}{L_p + L_s + L_n}$

Table B2
The definitions of variables in the P2D model.

Dependent variable name	Symbol
Li$^+$ concentration in electrolyte (mol m^{-3})	c_e
Solution phase current density (A m^{-2})	i_2
Potential in solution phase (V)	ϕ_2
Solid phase current density (A m^{-2})	i_1
Potential in solid phase (V)	ϕ_1
Surface reaction rate (mol m^{-2} s)	J
Open circuit potential (V)	U
Electrochemical overpotential (V)	η
Li concentration in solid phase (mol m^{-3})	c_s

Table B3
Parameter values for the P2D model.

Parameter	Value		
	Positive electrode	Separator	Negative electrode
Maximum Li capacity $c_{s,\text{max}}$ (mol m^{-3})	49,000		28,700
Radius of particle R_s (m)	5.0×10^{-6}		12.5×10^{-6}
Reference particle diffusion coefficient $D_{s,\text{ref}}$ (m^2 s^{-1})	3.0×10^{-15}		9.0×10^{-14}
Activation energy for particle diffusion Ea$_{di}$ (J mol^{-1})	4.0×10^3		2.0×10^4

Table B3 (*continued*)

Parameter	Value		
	Positive electrode	Separator	Negative electrode
Average electrolyte concentration $\bar{c}_e$ (mol/m^3)		1200	
Activity coefficient of solution phase $f_{\pm}$		0	
Thickness $l_p l_s l_n$ (m)	50×10^{-6}	25×10^{-6}	70×10^{-6}
Bruggeman factor β	2.0	2.0	2.0
Porosity $\varepsilon_p \varepsilon_s \varepsilon_n$	0.4	0.4	0.4
Volume fraction of active material ε_s	0.41		0.51
Specific surface area a (m^2 m^{-3})	2.66×10^5		1.02×10^5
Solid electronic conductivity σ (S m^{-1})	10		100
Reference reaction rate constant $k_{r,ref}$ (m$^{2.5}$ mol$^{0.5}$ s^{-1})	4.966×10^{-11}		7.773×10^{-10}
Activation energy for reaction Ea$_{re}$ (J mol^{-1})	3.0×10^4		3.0×10^4
The universal gas constant R (J mol^{-1} K)		8.314	
The Faraday constant F (C mol^{-1})		96,487	

References

[1] S. Browna, K. Ogawab, Y. Kumeuchic, S. Enomotoc, M. Unod, H. Saitod, Y. Soned, D. Abrahame, G. Lindbergha, J. Power Sources 185 (2008) 1444.
[2] M. Guo, R.E. White, J. Electrochem. Soc. 158 (10) (2011) A1166–A1176.
[3] V. Srinivasan, C.Y. Wang, J. Electrochem. Soc. 150 (1) (2003) A98–A106.
[4] G.-H. Kim, A. Pesaran, R. Spotnitz, J. Power Sources 170 (2) (2007) 476–489.
[5] S. Santhanagopalan, P. Ramadass, J. Zhang, J. Power Sources 194 (1) (2009) 550–557.
[6] U.-S. Kim, C.-B. Shin, C.-S. Kim, J. Power Sources 189 (1) (2009) 841–846.
[7] C.Y. Wang, V. Srinivasan, J. Power Sources 110 (2) (2002) 364–376.
[8] R.E. Gerver, J.P. Meyers, J. Electrochem. Soc. 158 (7) (2011) A835–A843.
[9] G.-H. Kim, K. Smith, K.-J. Lee, S. Santhanagopalan, A. Pesaran, J. Electrochem. Soc. 158 (8) (2011) A955–A969.
[10] K. Smith, C.-Y. Wang, J. Power Sources 161 (1) (2006) 628–639.
[11] K.A. Smith, C.D. Rahn, C.-Y. Wang, Energy Convers. Manage. 48 (2007) 2565–2578.
[12] V.R. Subramanian, V. Boovaragavan, V.D. Diwakar, Electrochem. Solid State Lett. 10 (11) (2007) 255–A260.
[13] V. Ramadesigan, V. Boovaragavan, J.C. Pirkle, V.R. Subramaniana, J. Electrochem. Soc. 157 (7) (2010) A854–A860.
[14] P.W.C. Northrop, V. Ramadesigan, S. De, V.R. Subramanian, J. Electrochem. Soc. 158 (12) (2011) A1461–A1477.
[15] M. Guo, R.E. White, J. Power Sources 198 (1) (2012) 322–328.
[16] M. Doyle, T. Fuller, J. Newman, J. Electrochem. Soc. 140 (6) (1993) 1526–1533.
[17] S. Santhanagopalan, Q. Guo, P. Ramadass, R.E. White, J. Power Sources 156 (2) (2006) 620–628.
[18] K. Kumaresan, G. Sikha, R.E. White, J. Electrochem. Soc. 155 (2) (2008) A164–A171.
[19] M. Guo, R.E. White, J. Power Sources 221 (1) (2013) 334–344.
[20] J. Newman, W. Tiedeman, J. Electrochem. Soc. 140 (7) (1993) 1961–1968.
[21] M. Chen, G.A. Rincon-Mora, IEEE Trans. Energy Convers. 21 (2) (2006) 504–511.

Glossary

$a_{c,+}, a_{c,-}$: specific electroactive surface area for current collectors, m^2 m^{-3}
A_c: cross-section area of electrode plates, m^2
$A_{\partial\Omega}$: area of boundary surfaces, m^2
C: rate capacity of cell, Ah
C_P: specific heat capacity of material, J K^{-1} kg^{-1}
$d_{c,+}, d_{c,-}$: thickness of current collectors, m
$d_{cell}, d_{Tab}, d_{BB}$: thickness of cell/tab/busbar, m
$h_{c,in}$: heat transfer coefficient in the spaces between cells, W m^{-2} K^{-1}
$h_{c,ext}$: heat transfer coefficient between battery and surroundings, W m^{-2} K^{-1}
i_N: normal inward current density, A m^{-2}
i_v: volumetric current source, A m^{-3}
I_{app}: current applied to or from the module, A
$\underline{\mathbf{k}}$: matrix for thermal conductivities, W K^{-1} m^{-1}
$\overline{k_c}$: thermal conductivity of material, W K^{-1} m^{-1}
k_{planar}: planar thermal conductivity of cell electroactive region, W m^{-1} K^{-1}
k_{transv}: transversal thermal conductivity of cell electroactive region, W m^{-1} K^{-1}
l_n, l_p, l_s: thickness of positive and negative electrode coatings and separator, m
n: normal unit vector pointing out of the boundary
N_d: number of double-sided positive electrode plates in cell
N_x, N_y, N_z: heat flux in the x, y, and z directions, W m^{-2}
N_θ: heat flux in the ξ_θ direction, W m^{-2}
Q_{ECh}: volumetric electrochemical heat source, W m^{-3}
Q_v: volumetric heat source, W m^{-3}
t: time, K
T: temperature, s
T^{ave}: volume-average temperature in the cell electroactive region, K
$T_{i,L}, T_{i,R}$: surface temperature of the left\right boundary of the ith cell, K
T_{amb}: ambient temperature, K
V_0, V_1, V_2, V_3: reference potentials at selected locations, V
V_{Ω_E}: volume of cell electroactive region, m^3
x, y, z: spatial coordinates, m
Δ_{Cell}: distance between two adjacent cells, m
ε_c: volume fraction of current collectors in the tab bases
$\varepsilon_{c,+}, \varepsilon_{c,-}$: volume fraction of current collectors in the cell electroactive regions
ε_e: volume fraction of electrode coatings and separator
Φ: electric potentials of busbar, V
Φ_+, Φ_-: electric potentials of current collectors, V
Φ_+, Φ_-: volume-average potentials in the cell electroactive region, V
Φ_L, Φ_R: modified potentials, V
θ: elevation angle for conductor foils in the tab base, rad
$\underline{\underline{\mathbf{\Theta}}}$: orientation matrix for anisotropic phase
ρ: density of domain material, kg m^{-3}
ρ_c: density of conductors, kg m^{-3}
$\underline{\underline{\mathbf{\sigma}}}$: matrix for electrical conductivities, S m^{-1}
$\overline{\sigma_c}$: electrical conductivity of material, S m^{-1}
ξ_θ: direction with an elevation angle of θ to the y axis
Ω_E: geometry domain for cell electroactive region
∇: the gradient operator, m^{-1}